J. Math. Biol. (1991) 29: 405–423

Journal of
Mathematical
Biology

On the dynamics of bursting systems

J. C. Alexander[1,] * and Da-Yong Cai[2,] **

[1] Department of Mathematics, University of Maryland, College Park, MD 20742, USA
[2] Department of Applied Mathematics, Tsinghua University, Beijing 100084, People's Republic of China

Received April 12, 1990; received in revised form June 15, 1990

Abstract. The dynamics of three-variable models of bursting are studied. It is shown that under certain conditions, the dynamics on the attractor can be essentially reduced to two dimensions. The salient dynamics on the attractor can thus be completely described by the return map of a section which is a logistic interval map. Two specific bursting models from the literature are shown to fit in the general framework which is developed. Bifurcation of the full system for one case in investigated and the dynamical behavior on the attractor is shown to depend on the position of a certain nullcline.

Key words: Bursting – Fast-slow decomposition – Bifurcation – Pancreatic β-cell model

1. Introduction

One of the interesting behaviors in cell-membrane models is bursting, in which a rapid oscillatory state alternates with a quiescent recovery state (Adams and Benson 1985; Alving 1968; Atwater et al. 1980; Chay 1985; Chay 1986; Chay and Keizer 1983; Chay and Rinzel 1985; Hindmarsh and Rose 1984; Johnson and Brown 1984; Plant 1978; Plant 1981; Plant and Kim 1976; Rinzel 1985; Traub 1982; Wong and Prince 1978; Wong and Prince 1981). Bursting has also been observed in chemical systems (DeKepper et al. 1976; Hudson et al. 1979; Hudson et al. 1986). A number of analyses on different aspects of the dynamics of bursting have been done (Alexander et al. 1989; Alexander et al. 1990; Argemi et al. 1984; Argemi et al. 1979; Argemi et al. 1980; Baer and Tier 1986; Decroly and Goldbeter 1987; Ermentrout and Kopell 1986; Honerkamp et al. 1985; Janz et al. 1980; Rinzel 1987; Rinzel and Lee 1986; Rinzel and Lee 1987; Rinzel and Troy 1982; Rinzel and Troy 1983; Terman 1989). In order to isolate essential aspects of bursting dyamics, simple bursting systems have been constructed, in particular 3-variable models. Essentially these models consist of two "fast" variables and one "slow" variable. If the slow variable is made infinitely

* Supported in part by N.S.F.
** On leave at University of Maryland

slow (by adjusting a time-scale parameter ε to 0) so that the system is degenerate, the resulting 2-dimensional system on the fast variables exhibits bistability; it can exist in a stable periodic state or a stable stationary state. When $\varepsilon \neq 0$, the slow variable moves the fast subsystem between the two states, resulting in the oscillatory and quiescent states.

In order to understand the dynamics of models, it is necessary to explain the observed behavior from basic features of the differential system. For example, Chay (1985), following earlier work on a larger model (Chay and Rinzel 1985), considered various delay and return maps of the model and realized them as interval maps. Similarly, Rinzel and Troy (1982) constructed a simplified model of Janz et al. (1980) of the Belousov–Zhabotinskii reaction. With an analysis of the return map, they were able to predict behavior of the model, such as multiple stable periodic orbits (Rinzel and Troy 1983). In both cases, the important dynamical behavior of the attractor—both regular and complicated—seems to be completely described by these interval maps. Since a return map is described by a one-dimensional map, the important dynamics on the full attractor should be described in two-dimensions. We seek to extract such an explanation from the dynamics of the original three-dimensional system. Terman (1989) has recently obtained some results in this direction. He shows that for certain 3-variable models which are sufficiently close to degeneracy (ε sufficiently close to 0), complicated dynamics can arise from the presence of a horseshoe in a return map. He presents an explicit example exhibiting this phenomenon. His result does not reduce the dynamics to two dimensions, since the horseshoe in the return map is itself two dimensional, and in the model he discusses, a further reduction is not possible. However, his underlying approach is the same as ours: determine the key dynamical behavior on the attractor in terms of the dynamics of the full system.

In this paper, we investigate the 3-variable models of Chay, Hindmarsh–Rose, and Rinzel–Troy. We show the dynamics on the attractor is essentially two-dimensional, and develop a general model for such a reduction of dimension. In particular, the return map is essentially a logistic interval map, and thus for certain values of the parameters, there is complicated dynamics. The full models satisfy conditions similar to, but slightly different from, those of Terman. However, where Terman finds horseshoes, we find one-dimensional dynamics, and in that sense, the dynamics of our model is simpler than those described by Terman. One of the systems we consider is Chay's model for the bursting of the pancreatic β-cell. Terman uses asymptotic analysis and his arguments are mathematically rigorous. The present paper discusses numerical examples that are not near the asymptotic limit and we do not achieve rigor. In particular, for our cases, the time-scale parameter ε is not small enough that we can appeal to such an asymptotic analysis for rigorous results. However, as discussed below, it is likely that a rigorous formalism can be constructed for the systems we consider; however, in addition to ε, a second degeneracy parameter must be incorporated.

We next indicate briefly the form of our model. More details are given in the next section. The model conforms to a rather standard model for regular bursting. We consider a 3-variable autonomous system

$$\dot{x} = f_1(x, y, z), \tag{1.1}$$

$$\dot{y} = f_2(x, y, z), \tag{1.2}$$

$$\dot{z} = \varepsilon f_3(x, y, z), \tag{1.3}$$

with fast variables x and y, and slow variable z. If $\varepsilon = 0$, the system is degenerate; it reduces to a two-dimensional system in x and y with z as parameter. The degenerate system has an S-shaped curve of stationary points. The lower branch of the S is stable and a family of stable periodic orbits "surrounds" the upper branch of the S (see Figs. 1, 2). The slow dynamics in z is such that for the non-degenerate system, the state varies between approximating the stable stationary state and the stable periodic state. As the system makes its transition from the former to the latter, it passes close to the unstable stationary point of the degenerate system in the middle branch of the S. Here it is trapped by the two-dimensional unstable manifold of the middle branch, which effectively reduces the number of degrees of freedom from three to two.

2. Chay's β-cell model

Chay and Keizer (1983), following the experimental work of Atwater et al. (1980), developed a model for the ionic and electrical behavior of the pancreatic β-cell. Chay (1985) reduced the model to three variables. In this section, we further the study of the dynamics of that model. The model is the following:

$$\dot{V} = g_I^* m_\infty^3 h_\infty (v_I - V) + g_{K,V}^* n^4 (V_K - V) + g_{K,C}^* \frac{C}{1+C}(V_K - V) + g_L^*(V_L - V), \tag{2.1}$$

$$\dot{n} = (n_\infty - n)/\tau_n, \tag{2.2}$$

$$\dot{C} = \varrho(m_\infty^3 h_\infty (V_C - V) - k_C C), \tag{2.3}$$

where

$$\begin{aligned}
\alpha_m &= 0.1(25 + V)/(1 - \exp(-0.1V - 2.5)),\\
\beta_m &= 4\exp(-(V + 50)/18),\\
m_\infty &= \alpha_m/(\alpha_m + \beta_m),\\
\alpha_h &= 0.07\exp(-0.05V - 2.5),\\
\beta_h &= 1/(1 + \exp(-0.1V - 2)),\\
h_\infty &= \alpha_h/(\alpha_h + \beta_h),\\
\alpha_n &= 0.01(20 + V)/(1 - \exp(-0.1V - 2)),\\
\beta_n &= 0.125\exp(-(V + 30)/80),\\
n_\infty &= \alpha_n/(\alpha_n + \beta_n),\\
\tau_n &= (\alpha_n + \beta_n)/230.
\end{aligned}$$

In this model, V is the difference of the external and internal voltages, n is a gating variable for K^+, and C is the Ca^{2+} concentration. Typical values for the parameters are: $V_K = 75$, $v_I = 100$, $V_L = -40$, $V_c = 100$, $g_{K,C}^* = 11$, $g_{K,V}^* = 1700$, $g_I^* = 1800$, $g_L^* = 7$, $k_c = 3.3/18$, $\varrho = 0.27$. Chay uses $g_{K,C}^*$ as a bifurcation parameter. At the parameter value $g_{K,C}^* = 11$, the dynamics is aperiodic, and we fix $g_{K,C}$ at that value.

The variable C is the slow variable, with ϱ the time-scale parameter. If $\varrho = 0$, we can regard the resulting degenerate system as a 2-variable system (2.1)–(2.2)

with C as an additional parameter, which can then be considered a bifurcation parameter. The bifurcation diagram of this system is exhibited in Fig. 1.[1] The vertical axis is V. There is an S-shaped curve of stationary points, and a Hopf bifurcation at $C \approx -0.361$ (which value is physiologically meaningless, but dynamically relevant). The maximum and minimum V values of the periodic orbits on the resulting branch are exhibited; the periodic branch terminates in an orbit homoclinic to the stationary point on the central stationary branch at $C \approx 0.447$. The stability of the branches is also indicated. The lower branch of the stationary S-curve is stable; the middle branch consists of saddle points and the upper branch to the right of the Hopf bifurcation consists of totally unstable stationary points. The uninteresting part of the curve to the left of the Hopf bifurcation consists of stable points. The periodic orbits are stable.

Figure 2 is a zoom of Fig. 1 with some additional information. A (partial) typical orbit of the full system (2.1)–(2.3) with the parameters above is superimposed. Also the nullcline of (2.3) is superimposed. We note two facts evident in Fig. 2. (a) The C-nullcline is above the homoclinic point on the middle stationary branch (and above the middle branch for some distance to the right of the homoclinic point). (b) The value $\varrho = 0.27$ is not particularly small. If the system is nearly degenerate ($\varrho \approx 0$), an orbit drops nearly vertically from the

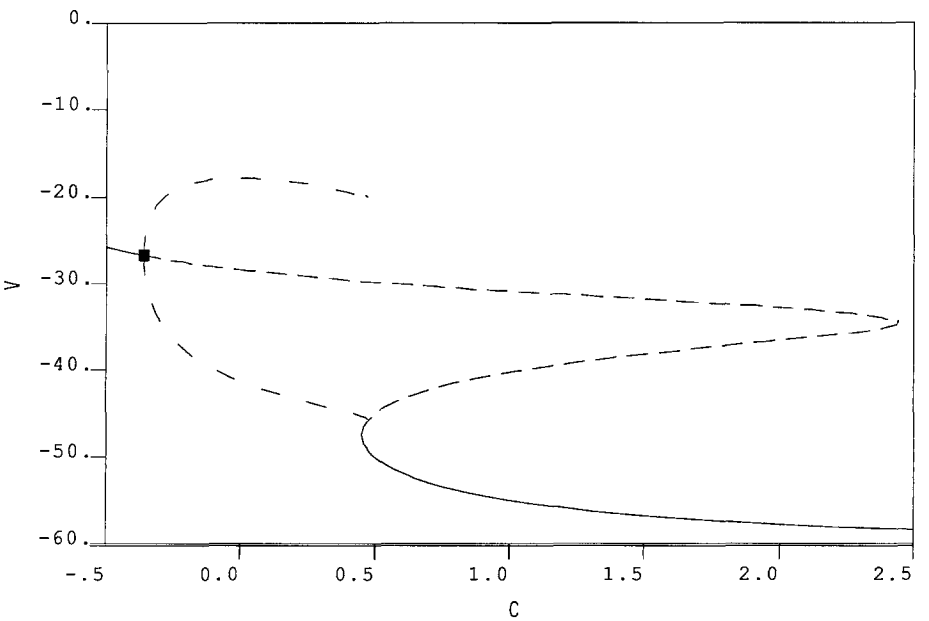

Fig. 1. Bifurcation diagram of (2.1)–(2.2), with C as bifurcation parameter. As discussed in text, there is an S-shaped curve of stationary points and a Hopf bifurcation (demarked by solid box) giving rise to a branch of periodic orbits. *Solid line*: stable stationary point; *dashed line*: unstable stationary points; *gapped dashed line*: upper and lower limits of stable periodic orbits

[1] Bifurcation diagrams in this paper were determined in double precision with the software AUTO (Doedel 1981); integrations were done in double precision with the ddriv routines in the software library cmlib

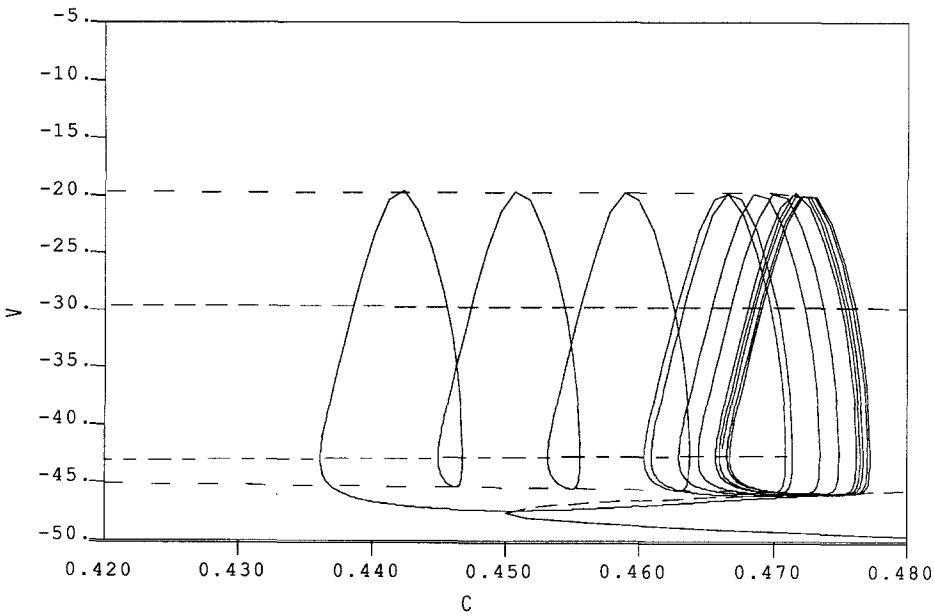

Fig. 2. Zoom of Fig. 1 with orbit of full system (2.1)–(2.3) and nullcline of (2.3) (*long-short dash*) superimposed

middle stationary branch to the lower branch. For the system as is, there is more horizontal than vertical movement in the lower part of an orbit.

Terman considers systems for which the corresponding degenerate system has the above form. Like him, we consider the return map of the flow descending through a plane $V = V_0$ just above the lower stationary branch of the degenerate system. Figure 3 exhibits the return map for system (2.1)–(2.3) for $V_0 = -46.5$. The important point here is that the points essentially lie on a one-dimensional submanifold—in this case a line. Indeed the best L^∞ (Chebyshev) fit is the line $C = 32.281n - 3.284$ with the maximal vertical deviation 2.6×10^{-6}. The deviation is 3.5 orders of magnitude smaller than the extent of the graph. The same holds if the axes are reversed. Consider the 3-variable degenerate system (2.1)–(2.3) with $\varrho = 0$. For each C for which there are three stationary points, the unstable manifold of the center stationary point is a 1-dimensional manifold which is separated into two components by the stationary point. Along one of them V decreases and descends to the lower stable stationary point. The union of these partial unstable manifolds is one component of the unstable manifold of the degenerate system (2.1)–(2.3). There is strong compression onto the unstable manifold. As an indication, near the homoclinic point, the eigenvalues of the linearization at the middle stationary point are approximately 10 and -35; orbits are compressed to the unstable manifold 3.5 times as fast as they are stretched out along it. Thus any orbit that comes near to the stable manifold leaves the region near the middle stationary point very close to the unstable manifold. For $\varrho > 0$, there are no stationary points and no stable or unstable manifolds. However there is still a compressive effect. Orbits of the non-degenerate system (2.1)–(2.3) are compressed towards a 2-dimensional surface. This is illustrated in Fig. 3; the intersections of the orbit with the plane $V = 46.5$ lie

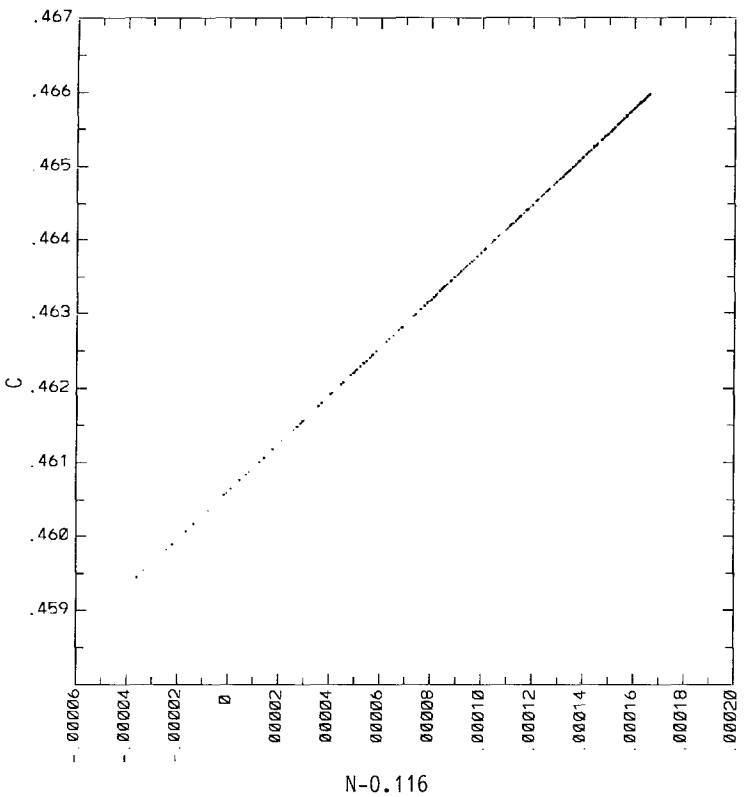

Fig. 3. Five hundred iterates of the return map of (2.1)–(2.3) on the plane $V = -46.5$. The n-axis has been shifted by 0.116. The points are virtually (i.e., to within two parts in 10^4) co-linear

virtually on the intersection of the surface with that plane. The fact that the intersection is almost a straight line is not particularly relevant; the fact that the intersection is 1-dimensional *is* relevant.

With this information, we construct our general model. We consider the 3-variable autonomous system (1.1)–(1.3), with fast variables x and y, and slow variable z (corresponding respectively to V, n, and C for Chay's model), such that the corresponding degenerate system ($\varepsilon = 0$) has the dynamics indicated in Fig. 2: an S-shaped set of stationary points which can be parameterized $y = s_2(x)$, $z = s_3(x)$ with $\lim_{x \to \pm\infty} s_3(x) = \mp\infty$, and with the indicated stability, and a branch of stable periodic orbits terminating at a homoclinic point $(x_\infty, y_\infty, z_\infty)$ on the center branch of stationary points. It is not necessary that the periodic orbits arise from a Hopf bifurcation, although that is usually the case. We are only interesting in the dynamics in a nieghborhood of the S-shaped curve. A single stable periodic orbit exists for each $z < z_\infty$ and the periodic orbit surrounds the upper stationary point. We consider the full 3-variable system with $\varepsilon > 0$. We suppose that for the full 3-variable system, the equation $f_3(x, y, z) = 0$ defines a surface which can be written $x = f(y, z)$. For $x < f(y, z)$, $f_3(x, y, z) < 0$ and vice versa. We suppose

$$f_3(x_\infty, y_\infty, z_\infty) < 0. \tag{2.4}$$

For $\varepsilon = 0$, the value of z does not change during the evolution of (1.1)–(1.3). Consider the periodic orbit $P_{\hat{z}}$ for (1.1)–(1.3) for $\varepsilon = 0$ with some value $z = \hat{z} < z_\infty$. Consider

$$L(\hat{z}) = \int_{P_{\hat{z}}} f_3(x, y, \hat{z})\, dt. \tag{2.5}$$

Let $T(\hat{z})$ denote the minimal period of $P_{\hat{z}}$. If $L(\hat{z})$ is positive, for ε small enough the orbit of (1.1)–(1.3) moves to the right (larger z). That is, if at time $t = 0$, an orbit starts at $(x, y, \hat{z})$ near $P_{\hat{z}}$, at time $T(\hat{z})$ the z value of the orbit is larger than $\hat{z}$. For negative $L(\hat{z})$, the opposite holds. This follows from the theory of averaging. By (2.4), $L(\hat{z}) < 0$ for $\hat{z}$ near z_∞. We assume there is $z_c < z_\infty$ such that $L(\hat{z}) > 0$ for $\hat{z} < z_c$ and $L(\hat{z}) < 0$ for $z_c < \hat{z} < z_\infty$.

We impose a second degeneracy in our model. We suppose there is a second parameter $\lambda \geqslant 0$ in (1.1)–(1.3) with the following effect. When $\varepsilon = 0$, there are 1-dimensional stable and unstable manifolds of the center branch stationary points. We suppose that for $\varepsilon = 0$, as $\lambda \to 0$, orbits in a neighborhood of the stable manifold on these points are collapsed onto the unstable manifold. Thus when λ is close to zero and ε is sufficiently small, orbits near the homoclinic point are still strongly compressed to a two-dimensional surface. This is the effect we observe in Fig. 3 for (2.1)–(2.3). In general, the parameter ε is explicitly in the differential equations, whereas λ is not and must be considered implicit. For the present paper, we do not try to develop mathematically precise notation and results.

We turn to the dynamic consequences of this model. Consider a section taken at a plane $X_{x_0} = \{(x, y, z) : x = x_0\}$ for a value of x_0 that is above the lower x-value of the periodic orbits of the degenerate system. For ε small, consider a point (x_0, y_0, z_0) with $z_0 < z_c$, where z_c is the point where $L(z)$ changes sign, and with $f_1(x_0, y_0, z_0) < 0$. Then the z-value, denote it z_1, of next descending return of the orbit to the plane is to the right of z_0. On the other hand, if $z_0 > z_c$, then $z_1 < z_0$. Suppose for no z_0 that $z_1 > z_\infty$. Then the orbit remains near the periodic orbits of the degenerate system and in fact approaches a periodic orbit. The return map $z_0 \mapsto z_1$ has a stable fixed point. This dynamic behavior of (2.1)–(2.3) is called *beating*. On the other hand, suppose there is some $z_0 < z_c$ such that the corresponding $z_1 > z_\infty$. Then the orbit "falls through" below the periodic orbits. It is caught in the compression of the previous paragraph, and the dynamics is essentially concentrated in a 2-dimensional attractor. If the attractor is 2-dimensional, a section is 1-dimensional. Thus representing the return map as an interval map is a complete description of the dynamics on the attractor. Note from Fig. 2, that the C-nullcline is near the V-minima of the periodic orbits so that z_c is close to z_∞, and hence bursting, rather than beating, occurs.

Consider the form of the return map on the plane X_{x_0}. We use z as the variable in the interval. Let $z_0, z_1, \ldots$ be the successive values. As discussed above, $z_{n+1} > z_n$ for $z_n < z_c$, and the return map is increasing. Consider the return of the interval $z > z_\infty$. Orbits descend below the periodic regime and are compressed to 2-dimensions. Note that in this region, $f_3(x, y, z) < 0$ so the motion is in the direction of decreasing z. The dynamics on the two-dimensional manifold is effectively a "rotation" as z decreases and inverts the z order (see Fig. 2). The return map is monotonically decreasing. Thus the return map has a logistic shape—monotonically increasing for small values of z and monotonically decreasing for large values of z. For $\varepsilon > 0$, this shape is preserved, except

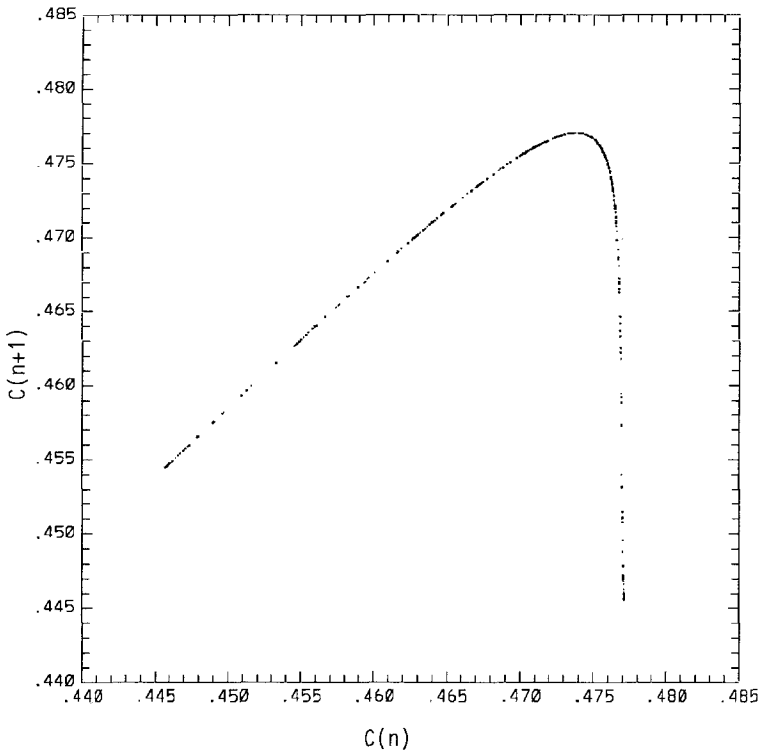

Fig. 4. The logistic return map of the C component for system (2.1)–(2.3) with parameters as given in the text. For these values the attractor is aperiodic and the return map samples most of the interval. The return map of the n-component is also logistic. This interval map captures the salient dynamics of the attractor

possibly near $z = z_\infty$, where the system is sensitive to perturbations. For the most part, however, the dynamics is essentially described by the logistic interval map.

It is well known that the logistic interval map admits complicated dynamics—period doubling cascades and aperiodic behavior. The details of the cascading depend on the shape of the graph of the return map at its maximum. When ε is very near 0, the maximum occurs for z very near z_∞, and the dynamics is the most sensitive to ε. That is, in the present model, the region of the graph near its maximum is the most sensitive to ε. Thus although the dynamics is described by an interval map, the detailed changes in the dynamics as a bifurcation parameter is varied may be difficult to quantify.

We return to the case of Chay's β-cell model. The return map for $V = -44$ is exhibited in Fig. 4. Note the logistic shape. Our model explains why the interval maps of Chay (1985) completely describe the dynamics of her model.

3. The Hindmarsh–Rose model

Hindmarsh and Rose (1984) have developed a three-variable model for the bursting of neurons, which is a variant of the Fitzhugh–Nagumo model

(Fitzhugh 1961). Much of their paper concerns the two-variable subsystem which describes the action potential. They add a third "adaptive" variable which is governed by a simple linear equation, and note that the resulting autonomous system admits aperiodic behavior. We consider this system in the context of the general model developed in the previous section.

The Hindmarsh–Rose model has three variables x, y, z, satisfying the following polynomial equations:

$$\dot{x} = y - ax^3 + bx^2 + I - z, \tag{3.1}$$

$$\dot{y} = c - dx^2 - y, \tag{3.2}$$

$$\dot{z} = r(s(x - x_1) - z). \tag{3.3}$$

For the physiological significance of the variables, the reader is referred to the original paper. The third variable is the slow variable and r is the time-scale parameter. Typical values for parameters are: $a = 1$, $b = 3$, $c = 1$, $d = 5$, $I = 0$, $I = 3.25$, $x_1 = -\frac{1}{2}(1 + \sqrt{5})$, $r = 0.005$, $s = 4$ (Hindmarsh and Rose 1984, p. 98).

If $r = 0$, so (3.3) is degenerate, there is an S-shaped branch of stationary points, as in Chay's model. The relevant portion of the bifurcation diagram of (3.1)–(3.2) is presented in Fig. 5. The branch of stable periodic orbits terminating in a homoclinic is present. There is also a smaller Hopf branch near the right-hand turning point. This branch is of some interest in its own right, as seen

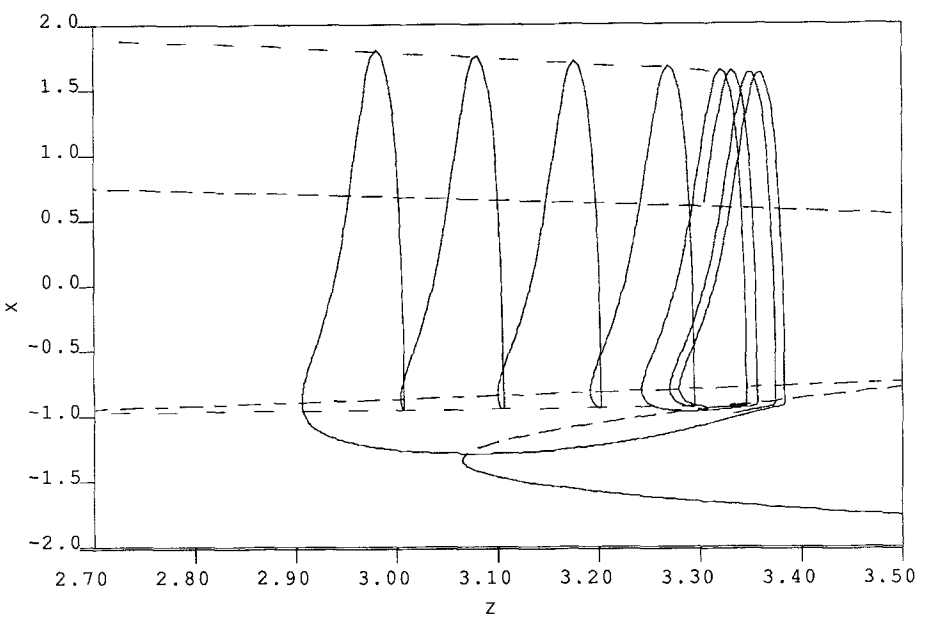

Fig. 5. Bifurcation diagram of (3.1)–(3.2), with parameters of the text, with z as bifurcation parameter. A bursting orbit of the full system (3.1)–(3.3) is superimposed. The nullcline of (3.3) is also superimposed. As in Figs. 1, 2 there is an S-shaped curve of stationary points and a Hopf bifurcation giving rise to a branch of periodic orbits. There is also a smaller Hopf branch near the right-hand turning point. This branch is not involved in bursting. *Solid line*: stable stationary point; *dashed line*: unstable stationary points; *gapped dashed line*: upper and lower limits of stable periodic orbits

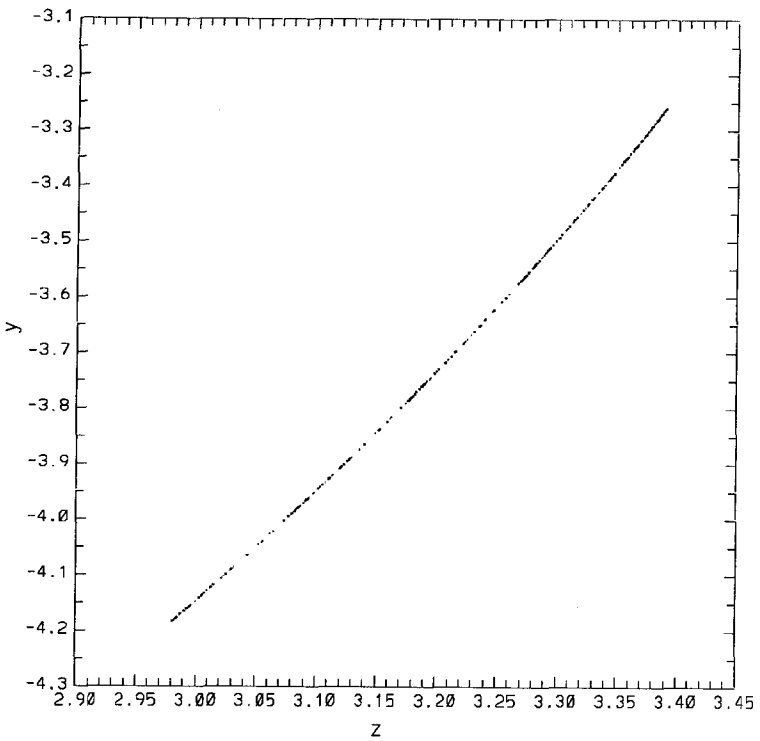

Fig. 6. Five hundred points of the return map of (3.1)–(3.3) on the plane $x = -0.85$. Again the points effectively lie on a one-dimensional set

below, but is not involved in the bursting phenomenon. A bursting orbit of the full system (3.1)–(3.3) is superimposed, as is the nullcline of (3.3). Note that the nullcline is above the homoclinic point.

Similarly, a section of the attractor is presented in Fig. 6. As in the case of Chay's model, the section is virtually a straight line, and in particular is 1-dimensional. Thus an interval map should describe the return map and as described in the previous section, the return map should be logistic. A return map for $x = -1$ is presented in Fig. 7. The logistic shape is clear.

4. The Rinzel–Troy model

Rinzel and Troy (1982) develop a simplified model of the Belousov–Zhabotinskii reaction with continuous flow-through. The equations are

$$\dot{y} = \frac{1}{s}(-y - g(y, r)y + f(p)z) - \frac{r}{s}y, \tag{4.1}$$

$$\dot{z} = w(g(y, r) - z) - \frac{r}{s}z, \tag{4.2}$$

$$\dot{p} = \frac{1}{s}\left(y + 2g(y, r)y + \frac{q}{2}(g(y, r))^2 - f(p)z\right) - \frac{\tau}{s}p, \tag{4.3}$$

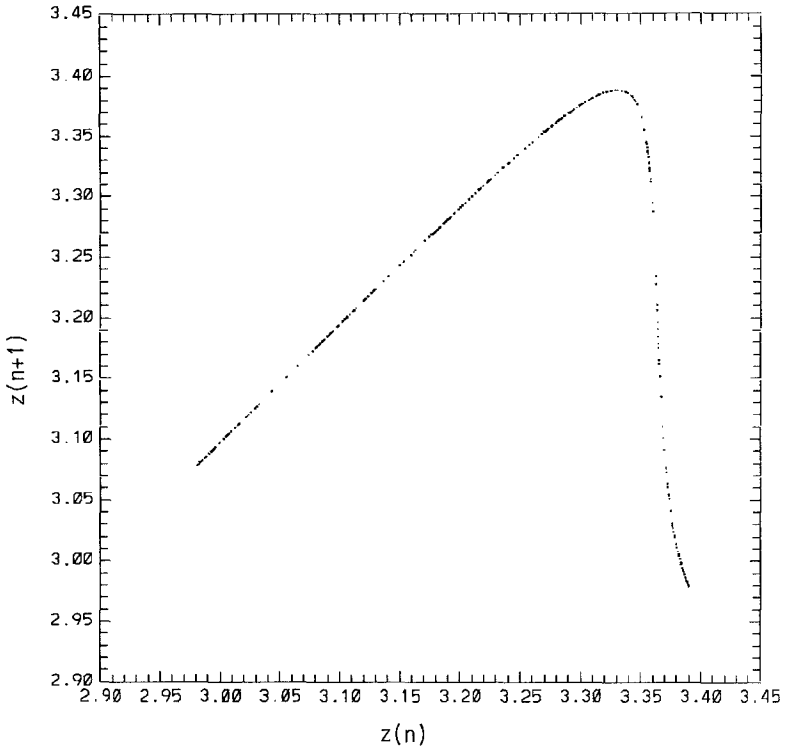

Fig. 7. The logistic return map of the z component for system (3.1)–(3.3) with parameters as given in the text with $z = -0.85$. For these values the attractor is aperiodic and the return map samples most of the interval. This interval map captures the complete dynamics of the attractor

where

$$g(y, r) = \frac{1}{2q}\left(1 - y - \frac{r}{s^2} + \left[\left(1 - y - \frac{r}{s^2}\right)^2 + 4q\left(y + \frac{rx^0}{s^2}\right)\right]^{1/2}\right),$$

$$f(p) = \frac{Fp^2}{K\bar{p}^2 + p^2} \quad \text{(the stoichiometric parameter)}.$$

The variables are concentrations of various chemicals. The third variable is the slow variable, although it is not evident from the form of (4.3). This set of equations is more complicated than (2.1)–(2.3) or (3.1)–(3.3) since $\dot{p}$ depends on both of the fast variables instead of only the first, and the behavior of the slow variable is more complicated. A more complete analysis will be presented elsewhere. Here we note only the behavior of the return map. Parameter values are $s = 77.27$, $w = 0.161$, $q = 8.375 \times 10^{-6}$, $F = 4$, $K = 0.0005$, $\bar{p} = 10^7/3$ and r (the flow rate) $= 0.00348985$. The return map to the plane $y = 2$ is exhibited in Fig. 8.

5. Discussion

We have developed a model that reduces the description of the dynamics on the attractor of a class of three-variable bursting models to logistic interval maps.

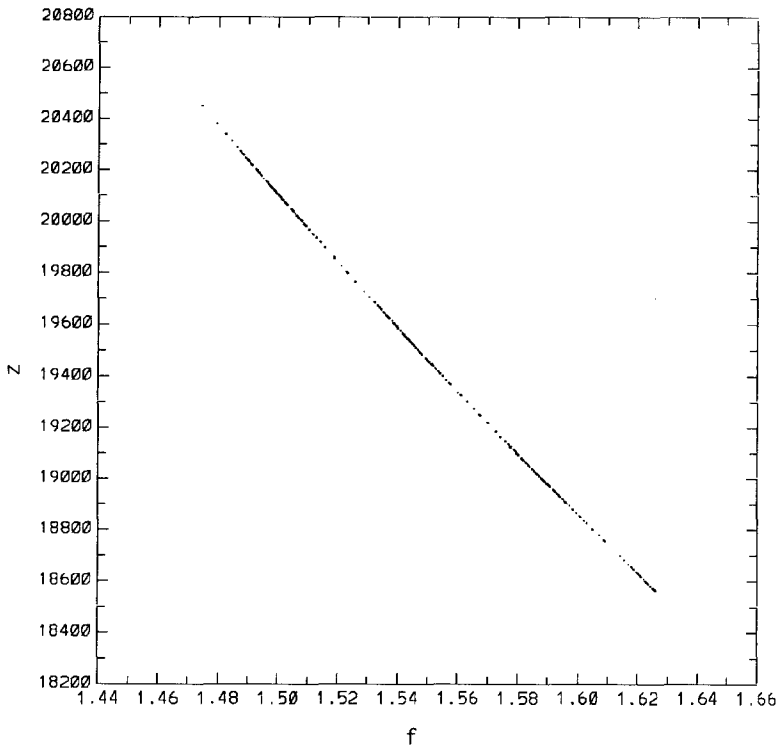

Fig. 8. Five hundred iterates of the return map of (4.1)–(4.3) on the plane $y = 2$

The key points of the model are: a fast-slow decomposition and a standard form for the dynamics if the slow system is infinitely slow and a compression of orbits towards a two-dimensional unstable manifold. A secondary feature is the influence of the position of the nullcline of the slow variable. In general of course, there will be very fine details in the dynamics which is not described by the interval map. However, it does describe the dynamical features salient to the physiology behind the model.

5.1. Terman's model

We contrast this model with that of Terman (1989). He also considers equations (1.1)–(1.3), and investigates the section on the attractor through a plane $z = z_0$ just above the lower stationary branch of the degenerate system. However, in contradistinction to us, he posits that the homoclinic point lies above the z-nullcline (his condition A6). Under this and his other conditions, there is a horseshoe in this return map. An essential condition for his result is that the z-nullcline lie below the homoclinic point. An important ingredient of this argument is an orbit that can "run up along" the middle stationary branch some distance towards the right-hand turning point before descending to the lower branch. Clearly, if the z-nullcline is above the homoclinic point, orbits that pass near to the homoclinic point must move to the left, not the right. Terman

considers the system

$$\dot{v} = y - 0.5(v + 0.5) - 2w(v + 0.7) - m_\infty(v)(v - 1),$$

$$\dot{w} = 1.15(w_\infty(v) - w)\tau(v),$$

$$\dot{y} = -\varepsilon[0.22 + v]\left[\left(\frac{\delta + 1}{2}\right) - \left(\frac{\delta - 1}{2}\right)\tanh\left(\frac{v + 0.23}{0.005}\right)\right],$$

with

$$M_\infty(v) = \frac{1}{2}\left[1 + \tan\left(\frac{v + 0.01}{0.15}\right)\right],$$

$$w_\infty(v) = \frac{1}{2}\left[1 + \tanh\left(\frac{v - 0.1}{0.145}\right)\right],$$

$$\tau(v) = \cosh\left(\frac{v - 0.1}{0.29}\right).$$

The parameter δ controls the relative speed of the dynamics on the lower stationary branch and upper periodic branch. For sufficiently small δ and ε, this system satisfies the conditions of Terman's theorem. The variable y is the slow variable. Terman exhibits the figure analogous to our Fig. 1. Note that the y-nullcline is the plane $v = -0.22$; this plane is below the homoclinic point and thus our description is not applicable. Terman also exhibits a section analogous to our Fig. 3; it is definitely two-dimensional.

In our model, it is λ, which governs the compression to the unstable manifold, which permits control of the dynamics. In fact, if λ is sufficiently small, so that there is sufficient compression, the model seems to be more robust in ε. This is the case in the models we consider. In general of course, there may be systems which exhibit behavior intermediate between that of Terman and ours. For these systems, a more complicated model will be necessary.

5.2. Bifurcation behavior of full model

A fuller picture of the dynamics can be developed by generating the bifurcation diagram for the full model. For her model, Chay has presented such a diagram using $g^*_{K,C}$ as bifurcation parameter (Chay 1985). Thus we concentrate on the Hindmarsh–Rose example. Since the location of the z-nullcline is important, we use x_1 as a bifurcation parameter for (3.1)–(3.3). Altering x_1 moves the z-nullcline vertically in Fig. 5 without changing its slope. The bifurcation diagram for the full system (3.1)–(3.3) with the parameters in the text is presented in Fig. 9, and a zoom in Fig. 10. Here the horizontal axis is x_1 and the vertical axis is x. For larger values of x_1, the z-nullcline is higher up. There is a branch of stationary orbits from lower left to upper right. There are four Hopf bifurcation points at x_1 values (zz) 3.904, (aa) -0.867, (bb) -1.064, and (ee) -2.077. In Fig. 12, the z-nullclines for the last three of these four values are superimposed on the graph of Fig. 5, along with some periodic orbits discussed below. Thus the intersection of the z-nullcline (ee) for Hopf point (ee) intersects

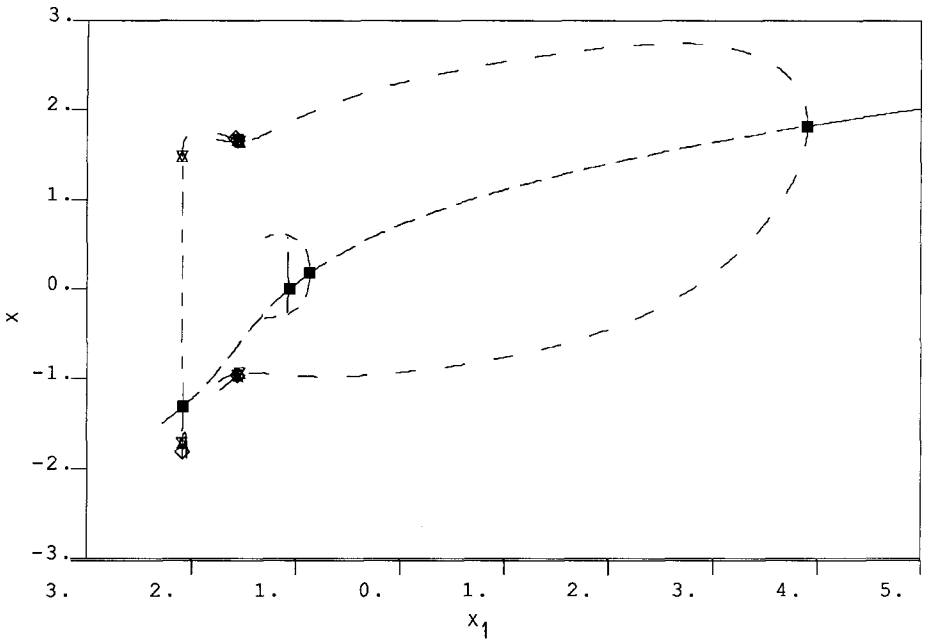

Fig. 9. Bifurcation diagram of (3.1)–(3.3), with x_1 as bifurcation parameter. The vertical axis is x. The figure is discussed in the text and clarified in the next three figures. There is a branch of stationary points from lower left to upper right. Hopf points are demarked with solid squares. Maxima and minima of periodic orbits are exhibited. *Solid line*: stable stationary point; *dashed line*: unstable stationary points; *gapped dashed line*: upper and lower limits of stable periodic orbits; *long-short dashed line*: upper and lower limits of unstable periodic orbits

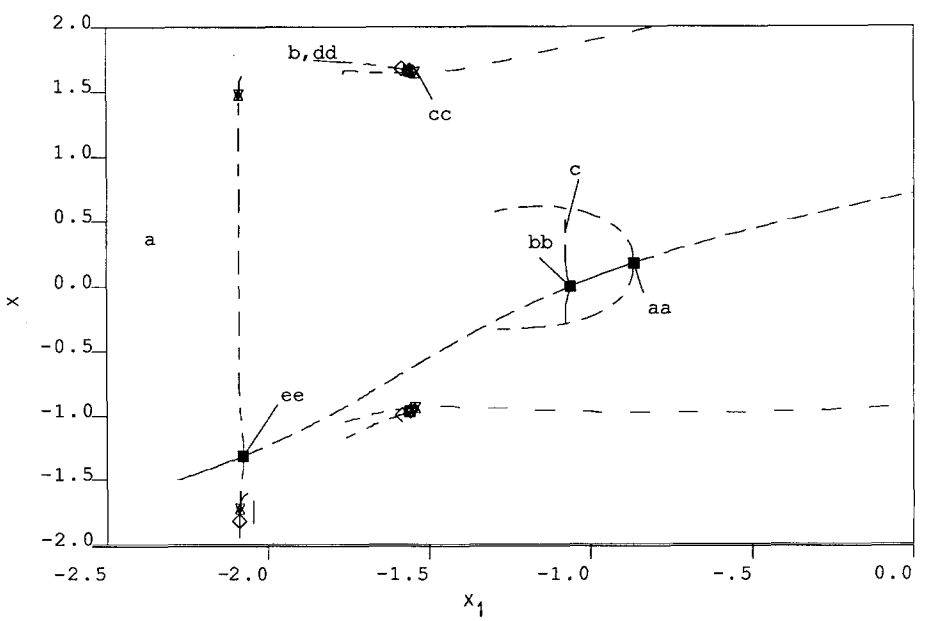

Fig. 10. Zoom of Fig. 9. Labels locate positions for next two figures

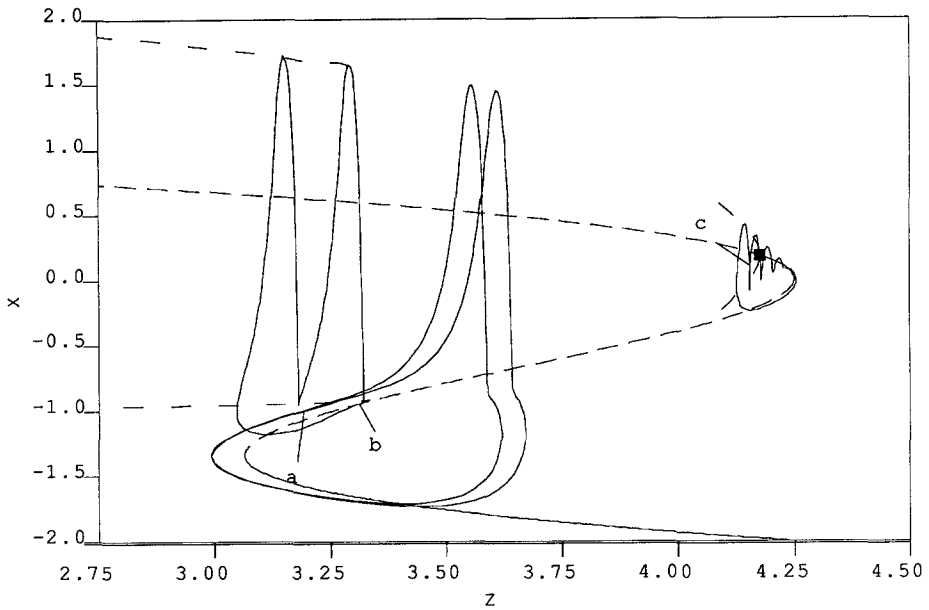

Fig. 11. Periodic orbits on the branches of Fig. 10 superimposed on the bifurcation diagram of Fig. 5. Labels correspond to positions in Fig. 10

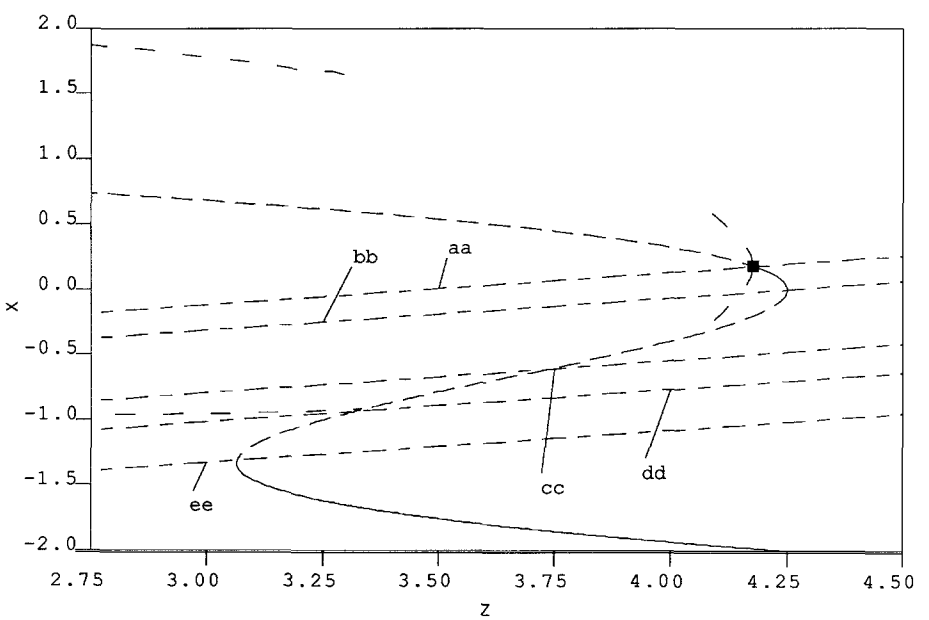

Fig. 12. z nullclines pertinent to Fig. 10 superimposed on the bifurcation diagram Fig. 5. Labels correspond to positions in Fig. 10. The nullclines: (aa) $x_1 = -0.867$, Hopf bifurcation point; (bb) $x_1 = -1.064$, Hopf bifurcation point; (cc) $x_1 = -1.544$, period doubling on periodic branch coming in from right; (dd) $x_1 = -1.767$, homoclinic terminus of periodic branch coming in from right; (ee) $x_1 = -2.077$, Hopf bifurcation

the S-curve of stationary points essentially at its left turning point. Similarly other Hopf points correspond to intersections with nullclines with other special points on the S-curve of stationary points.

From these Hopf points continua of periodic orbits branch. For each of these branches the maximum and minimum of x are shown in Fig. 9. The branch corresponding to bursting is the larger branch of periodic orbits orginating at the Hopf point (zz) at $x_1 = 3.904$. For much of the x_1 range, there is a single periodic orbit on this branch. At $x_1 = -1.544$, there is a period doubling. The nullcline (cc) of Fig. 12 is the one for this value of x_1. A second period doubling occurs at $x_1 = -1.560$ and a third at $x_1 = -1.564$. Presumably there is a period doubling cascade to the left of this point. It is in this region that true bursting occurs. A period-2 orbit from this branch is exhibited as orbit (b) in Fig. 11. Each of these branches seems to terminate at an unstable homoclinic. These homoclinics occur with $x_1 \approx -1.767$. The z-nullcline (dd) for this value is also plotted in Fig. 12. Note that it crosses the S-curve of stationary points very near the homoclinic point.

The branch emanating from Hopf point (ee) is subcritical. The periodic orbits branch to the left and are unstable. There is one period-doubling bifurcation from this branch at $x_1 = -2.089$ and possibly some others, all evidently unstable. A period-doubled orbit from this region is exhibited as orbit (a) in Fig. 11.

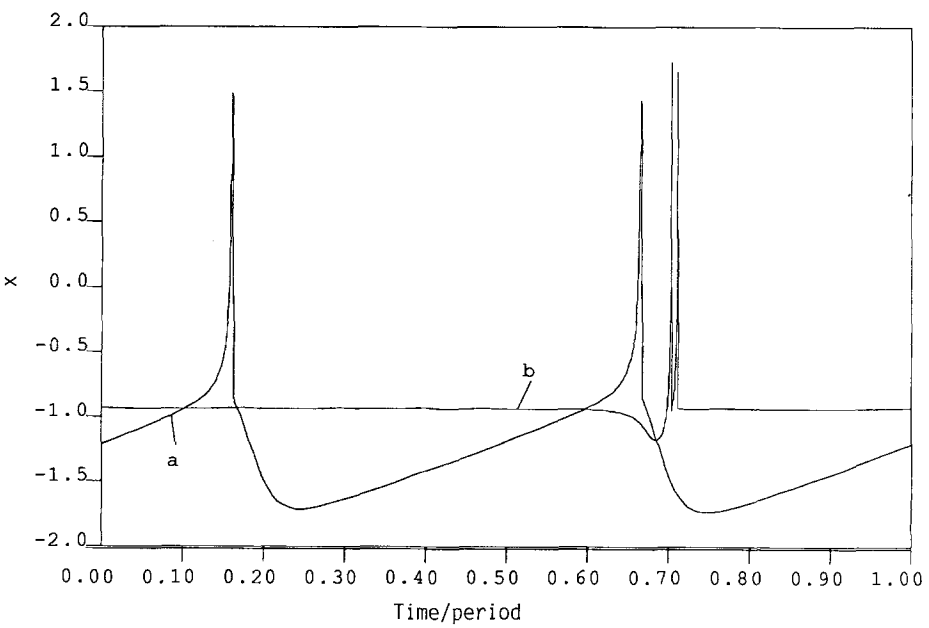

Fig. 13. The time traces of two period-doubled periodic orbits of (3.1)–(3.3) which are on branches of Fig. 10. These are the time traces of the correspondingly labelled orbits of Fig. 11. The horizontal axis is time normalized to 1 period. The actual periods of the two orbits are ≈ 460 and ≈ 2160, respectively. The vertical axis is x. The sharp spikes in the orbits prevent the software frrom following the branch further. However (a) is not close to homoclinic; if it were, there would be a long nearly horizontal tail at each end. Thus the leftmost branches do not terminate as indicated in Fig. 10. Orbit (b) is close to homoclinic, and the rightmost branches likely do terminate as indicated

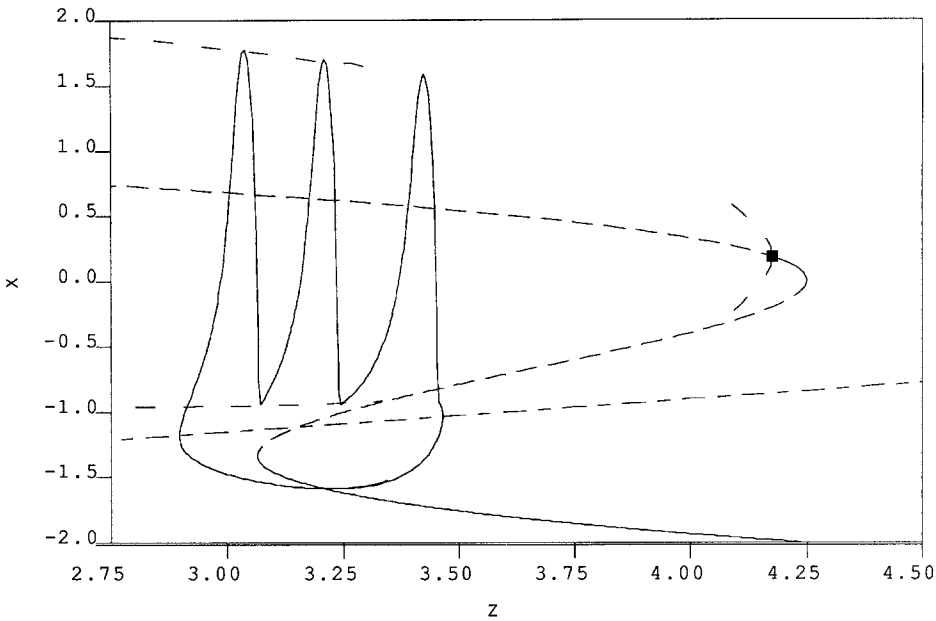

Fig. 14. A stable orbit for $x_1 = -1.9$ superimposed on the bifurcation diagram for (3.1)–(3.2), along with the corresponding nullcline of (3.3). Although this orbit is triply-spiked, it is not a period-3 orbit in the sense that orbit (a) in Fig. 11 is a period-2 orbit, and thus does not arise from the same kind of bifurcation behavior. It is more like orbit (b). *Solid line*: stable stationary point; *dashed line*: unstable stationary points; *gapped dashed line*: upper and lower limits of stable periodic orbits; *long-short dashed line:* nullcline of (3.3)

The Hopf bifurcations (aa) and (bb) are related to the rightmost branch of periodic orbits in Fig. 5. They are unrelated to bursting phenomena, but have some interest in their own right. The branch emanating from (aa) consists of unstable periodic orbits which are single loops in the phase space. The branch terminates in a homoclinic. The periodic orbits on the branch emanating from (bb) "wind around" many times as the z-value increases and then returns along the middle stationary branch. One of these orbits is exhibited as orbit (c) in Fig. 11. These orbits are stable, but with relatively small domains of attraction. The number of times the orbit winds around increases without bound as we move out the branch, as does the period, and in a suitable topology, the branch terminates on the branch from (aa). That is, this branch is an example of a branch with terminates by approaching a simple periodic orbit. The stationary points between (aa) and (bb) are stable.

It may be noted that there is a region between $x_1 \approx -2$ and $x_1 \approx -1.75$ in Fig. 10 with no stable stationary points and no exhibited periodic orbits of any kind. In fact, direct integration of (3.1)–(3.3) indicates there are stable periodic orbits in this region. They are probably on a continuation of a branch emanating from (ee). The orbits on these branches become very spiked and the software cannot follow the branch further; however there is no evidence the orbits are approaching a homoclinic. The time traces of orbits at the limits of two of the branches visible in Fig. 10 are exhibited in Fig. 13 (both are at the end of a computed period-doubled branch). These are the time traces of the correspond-

ingly labelled orbits of Fig. 11. An orbit with three spikes obtained by direct integration with $x_1 = -1.9$ is exhibited in Fig. 14. This orbit likely lies on a continuation of the left branch of Fig. 10; however it does not have the qualitative behavior of orbits on the left branch, and in fact is qualitatively closer to a bursting orbit. Note that in this range of x_1, the z-nullcline is below the homoclinic point. It is in this range of x_1 that a horseshoe might be found. We have not been able to pin down a non-periodic orbit to look for one. It is also by no means clear that the conditions of Terman are satisfied. The compressive effect is strong enough that the important aspects of the dynamics on the attractor remain 2-dimensional.

References

Adams, W. B., Benson, J. A.: The generation and modulation of endogenous rhythmicity in the Aplysia bursting pacemaker neuron R15. In Noble, D., Bundle, T. L. (eds.) Progress in biophysics and molecular biology, vol. 46, pp. 1–49. Elmsford, NY: Pergamon Press, 1985

Alexander, J. C., Doedel, E. J., Othmer, H. G.: Resonance of phase-locking in excitable systems. In: Othmer, H. G. (ed.) Some mathematical questions in biology: the dynamics of excitable media. (Lect. Math. Life Sci., vol. 21, pp. 7–37.) Am. Math. Soc., Providence, RI

Alexander, D. C., Doedel, E. J., Othmer, H. G.: On the resonance structure in a forced excitable system. SIAM J. Appl. Math. **50**, 1313–1418 (1990)

Alving, B. O.: Spontaneous activity in isolated somata of Aplysia pacemaker neurons. J. Gen. Physiol. **51**, 29–45 (1968)

Argemi, J., Chagneux, H., Ducreux, C., Gola, M.: Qualitative study of a dynamical system for metrazol-induced paroxysmal depolarization shifts. Bull. Math. Biol. **46**, 903–922 (1984)

Argemi, J., Gola, M., Chagneux, H.: Qualitative analysis of a model generating long potential waves in Ba-treated nerve cells—I. Reduced systems. Bull. Math. Biol. **41**, 665–686 (1979)

Argemi, J., Gola, M., Chagneux, H.: Qualitative analysis of a model generating long potential waves in Ba-treated nerve cells—II. Complete systems. Bull. Math. Biol. **42**, 221–238 (1980)

Atwater, I., Dawson, M., Scott, A., Eddlestone, G., Rojas, E.: The nature of oscillatory behavior in electrical activity for the pancreatic β-cell. J. Hormone Metabol. Res., Suppl. **10**, 100–107 (1980)

Baer, S. M., Tier, C.: An analysis of dendritic neuron model with an active membrane site. J. Math. Biol. **23**, 137–161 (1986)

Chay, T. R.: Chaos in a three-variable model of an excitable cell, Phys. D **16**, 233–242 (1985)

Chay, T. R.: Oscillations and chaos in the pancreatic β-cell. In: Othmer, H. G. (ed.) Nonlinear oscillations in biology and chemistry. (Lect. Notes Biomath., vol. 66, pp. 2–18.) Springer, Berlin–Heidelberg–New York, 1986

Chay, T. R., Keizer J.: Minimal model for membrane oscillations in the pancreatic β-cell. Biophys. J. **42**, 181–190 (1983)

Chay, T. R., Rinzel, J.: Bursting, beating, and chaos in an excitable membrane model. Biophys. J. **47**, 357–366 (1985)

DeKepper, P., Rossi, A., Pacault, A.: Etude experimentale d'une reaction chimique periodique. Diagramme d'etat de la reaction de Belousov–Zhabotinskii. C.R. Acad. Sci. Paris Sér. II Méc. Phys. Chim. Sci. Univers Sci. Terre C **283**, 371–375 (1976)

Decroly, O., Goldbeter, A.: From simple to complex oscillatory behavior: Analysis of bursting in a multiply regulated biochemical system. J. Theor. Biol. **124**, 219–250 (1987)

Doedel, E. J.: AUTO: A program for the automatic bifurcation and analysis of autonomous systems. Congr. Numer. **30**, 265–284 (1987)

Ermentrout, G. B., Kopell N.: Parabolic bursting in an excitable system coupled with a slow oscillation. SIAM J. Appl. Math. **46**, 233–253 (1986)

Fitzhugh, R.: Impulses and physiological states in theoretical models of nerve membrane. Biophys. J. **1**, 445–466 (1967)

Hindmarsh, J. L., Rose, R. M.: A model of neuronal bursting using three coupled first order differential equations. Philos. Trans. Roy. Soc. London Ser. **B221**, 87–102 (1984)

Honerkamp, J., Mutschler, C., Seitz, R.: Coupling of a slow and a fast oscillator can generate bursting. Bull. Math. Biol. **47**, 1–21 (1985)

Hudson, J. L., Hart, M., Marinko, D.: An experimental study of multiple peak periodic and non-periodic oscillations in the Belousov–Zhabotinskii reaction. J. Chem. Phys. **71**, 1601–1606 (1979)

Hudson, J. L., Lamba, P., Mankin, J. C.: Experiments on low-amplitude forcing of a chemical oscillator. J. Phys. Chem. **90**, 3430–3434 (1986)

Janz, R. D., Vanacek, D. J., Field, R. J.: Composite double oscillation in a modified version of the oregonator model of the Belousov–Zhabotinsky reaction. J. Chem. Phys. **73**, 3132–3138 (1980)

Johnson, D., Brown, T. H.: Mechanisms of neuronal burst generation. In: Schwartzkroin and H. V. Wheal (eds.) Electrophysiology of epilepsy, pp. 277–301. New York: Academic Press, 1984

Plant, R. E.: The effects of calcium on bursting neurons. J. Neurophys. **21**, 217–237 (1978)

Plant, R. E.: Bifurcation and resonance in a model for bursting nerve cells. J. Math. Biol. **11**, 11–32 (1981)

Plant, R. E., Kim, M.: Mathematical description of a bursting pacemaker neuron by a modification of the Hodgkin–Huxley equations. Biophys. J. **16**, 227–244 (1976)

Rinzel, J.: Bursting oscillations in an excitable membrane model. In: Sleeman, B. D., Jarvis R. J. (eds.) Ordinary and partial differential equations proceedings of the eight conference held at Dundee, Scotland, June 25–29, 1984. (Lect. Notes Math., vol. 1151, pp. 304–316.) Springer, Berlin–Heidelberg–New York, 1985

Rinzel, J.: A formal classification of bursting mechanisms in excitable systems. In: Proceedings of the International Congress of Mathematics, vol. 2, pp. 1578–1593. American Mathematical Society, Providence, RI, 1986

Rinzel, J., Lee, Y. S.: On different mechanisms for membrane potential bursting. In: Othmar, H. G. (ed.) Nonlinear oscillations in biology and chemistry. (Lect Notes Biomath., vol. 66, pp. 19–33.) Springer, Berlin–Heidelberg–New York, 1986

Rinzel, J. Lee, Y. S.: Dissection of a model for neuronal parabolic bursting. J. Math. Biol. **25**, 653–675 (1987)

Rinzel, J., Troy, W. C.: Bursting phenomena in a simplified Oregonator flow system model. J. Chem. Phys. **76**, 1775–1789 (1982)

Rinzel, J., Troy, W. C.: A one-variable map analysis of bursting in the Belousov–Zhabotinskii reaction. Cont. Math. **17**, 411–427 (1983)

Terman, D.: Chaotic spikes arising from a model of bursting in excitable membranes, Ohio State University, preprint (1989)

Traub, R. D.: Simulation of intrinsic bursting in CA3 hippocampal neurons. Neuroscience **7**, 1233–1242 (1982)

Wong, R. K. S., Prince, D. A.: Participation of calcium spikes during intrinsic burst firing in hippocampal neurons. Brain Res. **159**, 385–390 (1978)

Wong, R. K. S., Prince, D. A.: After potential generation in hippocampal pyramidal cells. J. Neurophysiol. **45**, 89–97 (1981)